Paleozoic amphibolite–granulite facies magmatic complexes in the hinterland of the Uralide Orogen

Article *in* International Journal of Earth Sciences · June 2000

DOI: 10.1007/s005310050315

CITATIONS
29

READS
64

4 authors, including:

Alexander Larionov
A.P. Karpinsky Russian Geological Research Institute
172 PUBLICATIONS **2,938** CITATIONS
SEE PROFILE

Georg. Askoldovich Petrov
Institute of Geology and Geochemistry, Uralian Geological Survey Expedition
67 PUBLICATIONS **311** CITATIONS
SEE PROFILE

David G. Gee
Uppsala University
194 PUBLICATIONS **5,977** CITATIONS
SEE PROFILE

Int J Earth Sci (2000) 89:21–39

ORIGINAL PAPER

M. Friberg · A. Larionov · G. A. Petrov · D. G. Gee

Paleozoic amphibolite–granulite facies magmatic complexes in the hinterland of the Uralide Orogen

Received: 7 May 1999 / Accepted: 2 November 1999

Abstract Within the hinterland of Urals, there occur a variety of high-grade complexes that have been interpreted to be fragments of continents that were accreted to Baltica during Paleozoic orogeny. Some workers have inferred the high-grade complexes to have rifted off Baltica during the Early Paleozoic; others claim that they were derived from elsewhere (perhaps Siberia) and are truly exotic terranes. In the Middle Urals, the amphibolite- to granulite-facies complexes of "micro-continental" affinities are generally composed of mafic to intermediate gneisses, overlain by Paleozoic mélange and island-arc volcanics. New Pb–Pb single zircon dating provides evidence only of a Paleozoic history for one of these high-grade units, the Salda Metamorphic Complex. Eight intrusion ages have been obtained from these granulite-facies gneisses and younger intrusions. The protoliths of the gneisses, the Teliana and the Brodovo intrusive suites, were formed at around 350 Ma (359 ± 5, 357 ± 7 and 343 ± 9 Ma) and at 393 ± 5 Ma, respectively. They are cut by the East Emekh granite (334 ± 4 Ma) and the Basianovo gabbro (336 ± 2 Ma). The new single zircon data fit well with previously conventional K–Ar, Pb–Pb and U–Pb ages by A.P. Grevtsova et al. (unpublished data). It is proposed here that the hinterland of the Middle Urals is dominated by Devonian to Middle Carboniferous subduction-related magmatic complexes that were emplaced prior to and during collisional orogeny in the Urals. The evidence presented here and age-data from other hinterland high-grade complexes casts doubt on the "micro-continent" interpretation.

Key words Ural Mountains · Paleozoic · Single zircon Pb/Pb evaporation ages · Hinterland metamorphic complexes · Russia

M. Friberg (✉) · A. Larionov · D. G. Gee
Department of Geophysics, Uppsala University, Villavägen 16, S-752 36 Uppsala, Sweden
Tel.: +46-18-4713325
Fax: +46-18-501110
e-mail: mf@geofys.uu.se

G. A. Petrov
Urals Geological Survey Expedition, UGSE, 55 Veinera., Ekaterinburg, Sverdlovsk, District 620014, Russia

Introduction

The Ural mountains are the remnants of Late Paleozoic collision between Baltica and outboard Kazakh and Siberian terranes (Hamilton 1970; Ivanov et al. 1975; Sengör et al. 1993). Within the hinterland of the mountain belt, high-grade metamorphic complexes underlie ophiolite mélange and volcanic-arc assemblages. The metamorphic complexes are dominated by deformed magmatic suites. They have been interpreted by most previous authors as fragments of old continental crust, e.g. Krasnobayev (1986), accreted to the margin of the Baltica during Late Paleozoic orogeny. This view has been questioned in recent years and new isotope age data presented here indicate that, at least in the Middle Urals (the Salda Metamorphic Complex), they represent middle and lower crustal segments of Paleozoic magmatic arcs.

In this paper we use the time scale proposed by Snelling (1985) and modified by Tucker and McKerrow (1995) to correlate stratigraphic and radiometric ages.

Geological overview

The Uralide orogen has traditionally been split into six N/S-trending tectonic zones (Fig. 1), from west to east: the Urals Foredeep, West Urals, Central Urals, Tagil-Magnitogorsk, East Uralian and the Trans-Uralian zones. The first three zones correspond to the foreland fold and thrust belt, involving the Precambrian basement of Baltica, Upper Proterozoic mainly

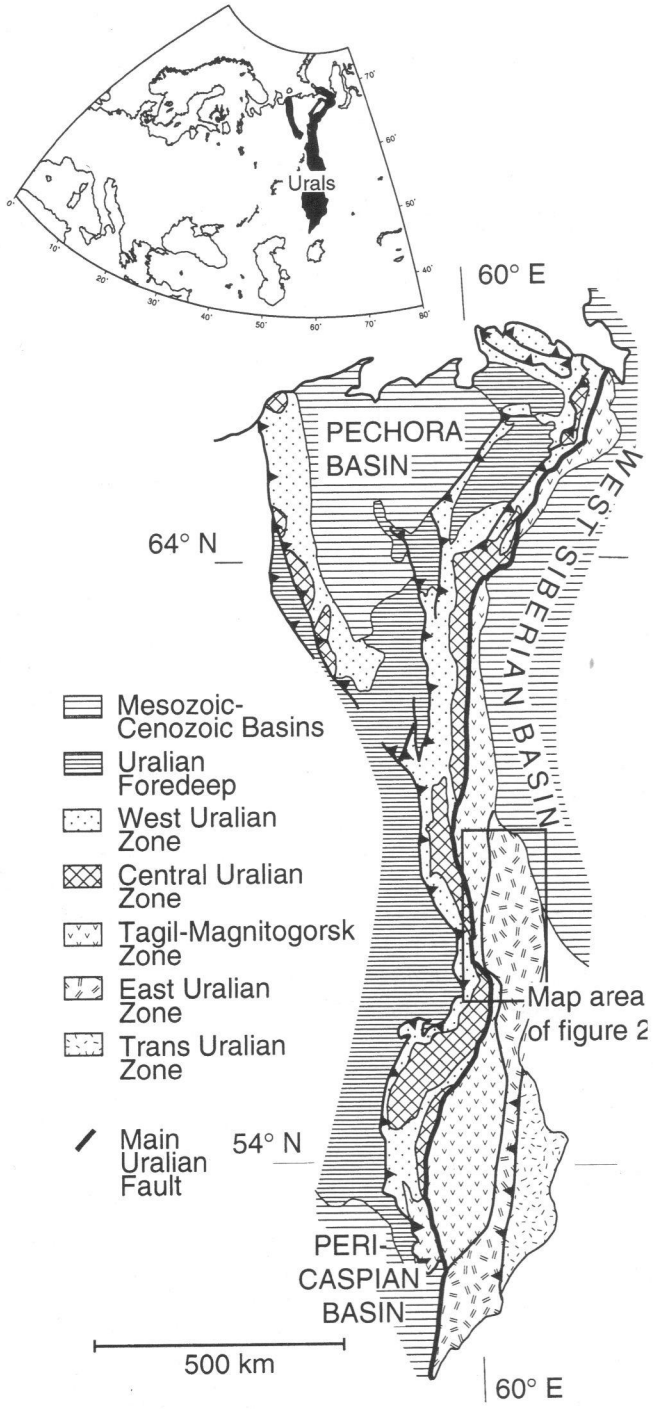

Fig. 1 Geological zones of the Urals Mountains. (Modified from Juhlin et al. 1998)

sedimentary sequences and unconformably overlying Paleozoic shelf and platform deposits. Further east and separated by a suture, commonly coincident with the Main Uralian Fault, is the Tagil-Magnitogorsk Zone which consists of well preserved Silurian and Devonian island-arc rocks and subordinate Ordovician ophiolite sequences (Antsigin et al. 1994). The East Uralian and Trans-Uralian zones, further towards the hinterland, consist of a collage of accreted terranes, intruded by late tectonic, Late Carboniferous to Early Permian plutons.

The Ordovician to Early Carboniferous Trans-Uralian island arc rocks and associated ophiolites, recognized in the Southern Urals, have not yet been identified in the Middle Urals and only the Ordovician to Silurian Tagil Volcanic Arc Complex (Friberg and Petrov 1998) of the Tagil-Magnitogorsk Zone is present here.

The East Uralian Zone of the Middle Urals

In the East Uralian Zone of the Middle Urals, there are two separate volcanic arc terranes: the Middle Silurian to Early Devonian Petrokamensk and the Silurian to Early Carboniferous Alapaevsk volcanic arc complexes; the latter is overlain by Carboniferous shallow water marine and continental sediments. The Petrokamensk and Alapaevsk complexes, such as the Tagil Volcanic Arc Complex, are underlain by mélange units consisting of serpentinite together with Devonian and older metasediments (Fig. 2). At deeper structural levels, high-grade metamorphic complexes are exposed in the cores of major N/S-trending antiforms and are intruded by Late Carboniferous to Permian granitoids (Sobolev et al. 1964; Fershtater et al. 1997).

Four high-grade terranes have been identified in the East Uralian Zone of the Middle Urals: the Salda, Murzinka-Adui, Sisert (Fig. 2) and Krasnogvardeiskii metamorphic complexes. The three first complexes consist mostly of mafic and felsic gneisses, ranging in metamorphic grade from upper amphibolite- to granulite-facies, locally retrograded to greenschist facies. The Krasnogvardeiskii Metamorphic Complex consists of granitic gneisses, largely covered by Mesozoic sediments and only exposed in a few outcrops near the Krasnogvardeiskii village (120 km northeast of Ekaterineburg). Previous studies, e.g. Keilman (1974), Antsigin et al. (1994), with a few exceptions (A.P. Grevtsova et al., unpublished data), have considered these terranes to be micro-continents largely composed of Proterozoic and/or Archean crust. However, recent work, both further south in the orogen (Echtler et al. 1997) and in the area considered here (Friberg et al. 1997; Friberg and Petrov 1998), has questioned the age of the supposed "Precambrian" terranes in the hinterland areas.

The East Uralian Zone is separated from the Tagil Volcanic Arc Complex by a steeply west-dipping shear zone, the Serov-Mauk Fault. The latest movement on this fault was normal with a sinistral component and it juxtaposes low-grade volcanics of the Tagil Volcanic Arc Complex in the hangingwall with amphibolite- and granulite-facies gneisses of the Salda Metamorphic Complex in the footwall (Figs. 3, 4). The Salda

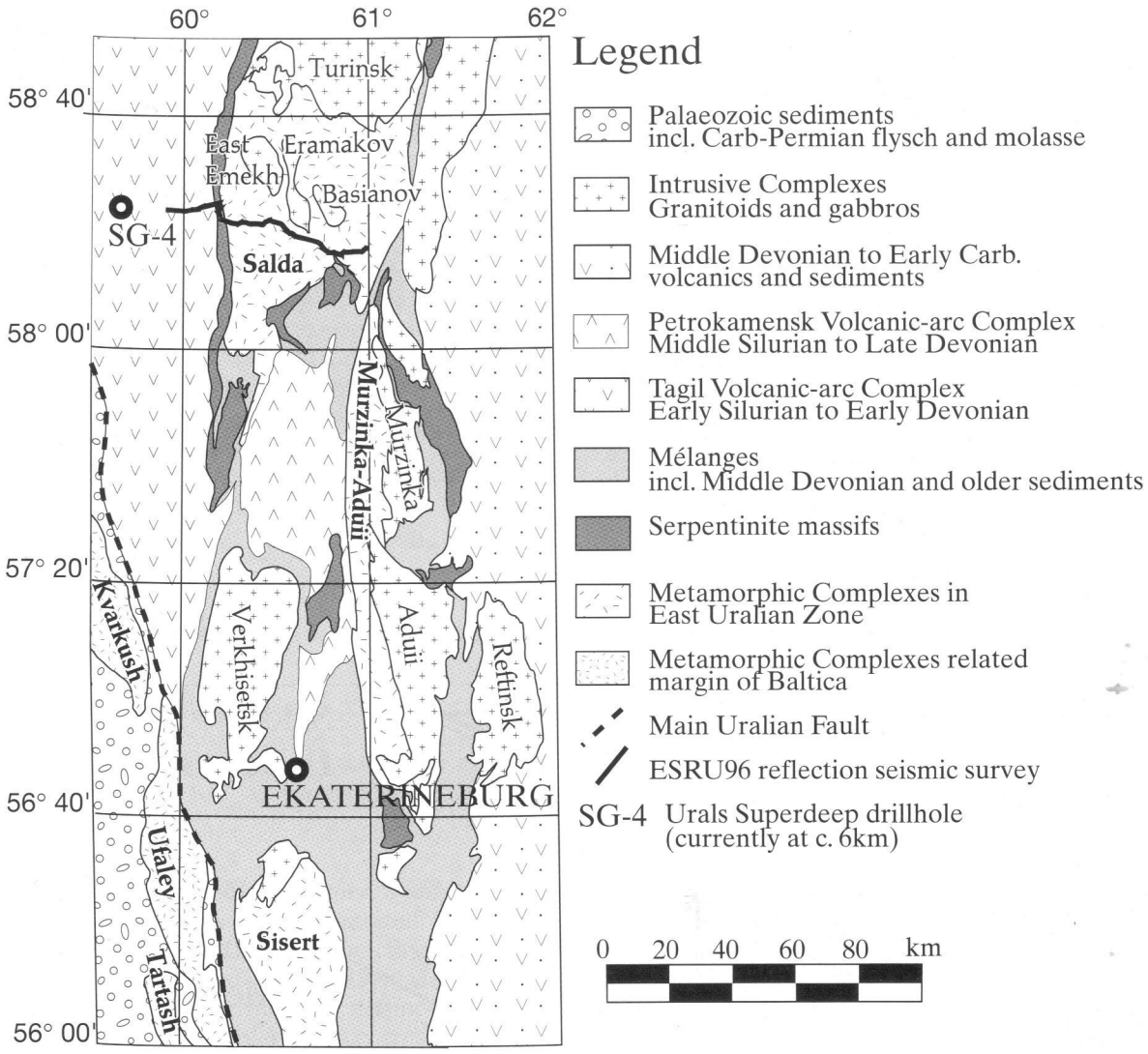

Fig. 2 The main tectonic elements in the Middle Urals

Metamorphic Complex is interpreted to have been thrust eastwards onto the Murzinka-Adui Metamorphic Complex along an approximately 35° west-dipping fault (Fig. 3). Both faults can be traced through the upper crust in the ESRU96 reflection seismic section (Juhlin et al. 1998).

The high-grade gneisses and the volcano-sedimentary rocks of the hinterland complexes are cut locally by subduction-related, Carboniferous (Rb–Sr mineral isochron ages of 316 ± 6 and 320 ± 12 Ma) tonalite, trondhjeimite and granodiorite (TTG) intrusions and Early Permian (Rb–Sr ages of 276 ± 5 and 284 ± 16 Ma) post-collisional granodiorites, adamellites and granites (Bea et al. 1997; Fershtater et al. 1997). Bea et al. (1997) demonstrate from field relationships, together with isotope and trace element studies of the Verkhisetsk batholith (Fig. 2), that the Permian granitoids are derived by partial melting of the TTG intrusions and that this occurred at moderate crustal levels ($P \approx 4$ kbar).

The main lithologies of the Murzinka-Adui Metamorphic Complex are orthogneisses derived from granodiorite and subordinate gabbro, cut by the Murzinka and Adui granitoids, which are most probably related to the Permian post-collisional granitoids (Fershtater 1993; Fershtater et al. 1997). The Murzinka-Adui gneisses have been considered to be of Riphean age (Sobolev et al. 1964; Antsigin et al. 1994), an interpretation based on their metamorphic grade and deep structural level. Conventional U–Pb zircon studies made in the 1960s (A.P. Grevtsova et al., unpublished data) on the gneisses have yielded upper intercept ages of 910 ± 60, 470 ± 50, 465 ± 30, 360 ± 40, 315 ± 30 and two samples at 260 ± 24 Ma. Whole rock K–Ar ages range from 340 to 175 Ma (A.P. Grevtsova et al., unpublished data).

The Sisert Metamorphic Complex was described by Keilman (1974) as having a core of granulite- and upper amphibolite-facies felsic and mafic gneisses,

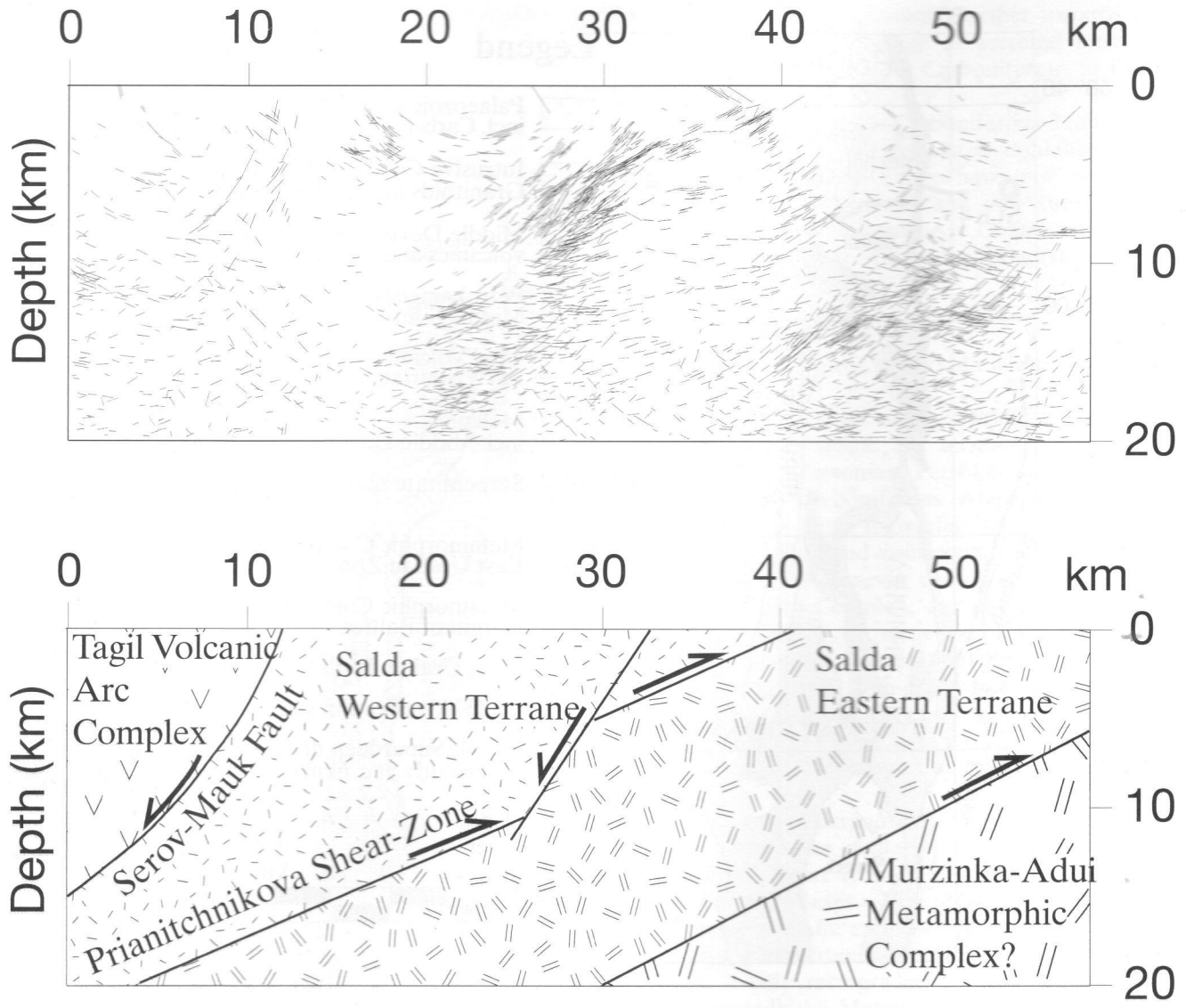

Fig. 3 **a** The migrated upper 6 s of the ESRU96 (Juhlin et al. 1998) reflection seismic survey, acquired across much of the Salda Metamorphic Complex. **b** Interpretation of the ESRU96 seismic survey. (Modified from Juhlin et al. 1998)

overlain by graphite-bearing paragneisses with lenses of gabbro amphibolites and serpentinites; the latter were interpreted to be composed of a part of an ophiolite sequence. Recent structural analysis, isotope and microprobe investigations of the Sisert Metamorphic Complex by Echtler et al. (1997) demonstrate that the high-grade gneisses are of Paleozoic age. U–Pb zircon multi-grain analyses yielded two groups of discordant upper intercept ages; the one Ordovician (between 437 ± 32 and 482 ± 41 Ma) and the other Early Carboniferous (355 ± 5 Ma) for the felsic gneisses; the older was interpreted to be the age of crystallization and the younger to be the age of metamorphism. The Carboniferous ages are in agreement with Sm–Nd ages (355 ± 40 Ma) from the same unit, and the Ordovician ages with a Rb–Sr whole-rock isochron (435 ± 33 Ma). The P–T determinations, based on microprobe analyses, indicate pressures of metamorphism between 6 and 8 kbar and temperatures as high as 700 °C (Echtler et al. 1997).

Salda Metamorphic Complex

The work reported here focuses on the Salda Metamorphic Complex, in the East Uralian Zone. It is part of a geological programme complementary the seismic profiling that started in 1992 (Juhlin et al. 1993). The ESRU96 (Europrobe Seismic Reflection in the Urals 1996) deep reflection seismic survey (Juhlin et al. 1998) crosses the Salda Metamorphic Complex and, in order to interpret the seismic section and the tectonic evolution, it was considered important to establish the age of the gneiss complex and its relation to the overlying island-arc volcanics.

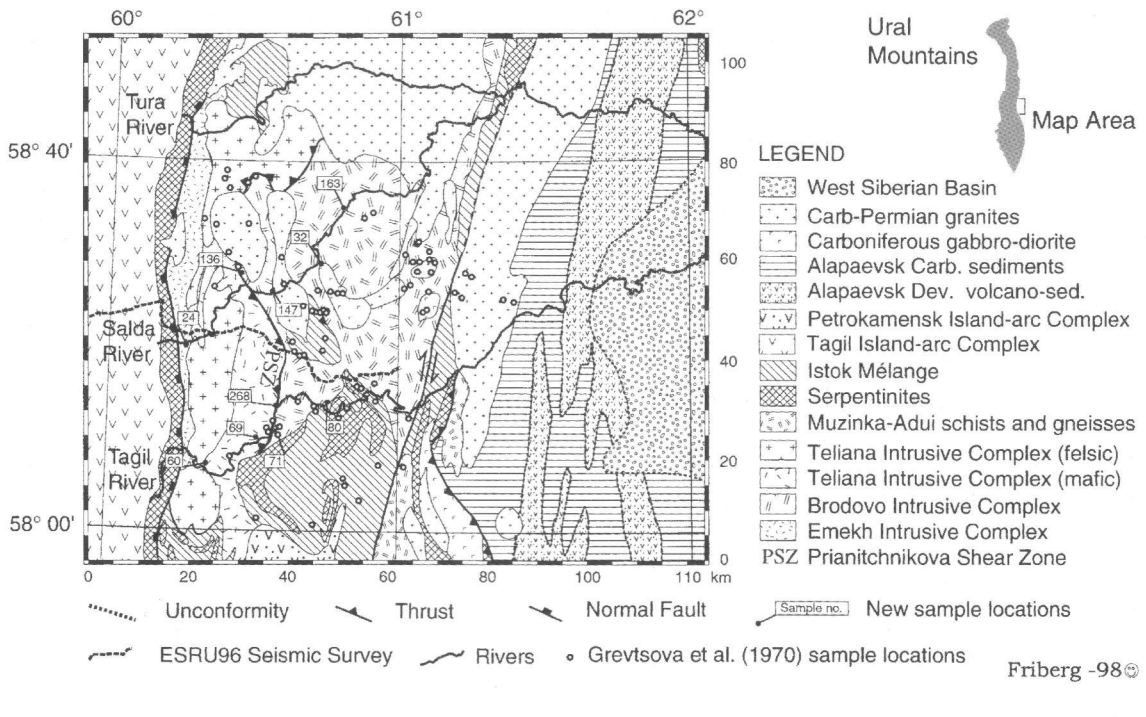

Fig. 4 The hinterland of the Middle Urals. Numbered location points are from this work; others are from A.P. Grevtsova et al. (unpublished data). The coordinates of Table 1 refer to the kilometer grid in this figure

The Salda Metamorphic Complex consists of two terranes (eastern and western) separated by a major west-dipping fault (Figs. 3, 4), the Prianitchnikova Shear Zone (Friberg and Petrov 1998; Juhlin et al. 1998). The Western Terrane is composed of the Emekh gneisses of probable oceanic crust, consisting predominantly of mafic to ultramafic gneisses of amphibolite- to granulite facies, locally with a greenschist-facies overprint. They are intruded by the Teliana granulite- to amphibolite-facies gabbro–diorite–granodiorite–plagiogranite suite (Keilman 1974; Petrov 1995; Friberg and Petrov 1998), which shows very little deformation, except near the shear zone.

The Eastern Terrane is dominated by granulite- and upper amphibolite-facies mafic and felsic orthogneisses of the Brodovo intrusive suite (Petrov et al. 1998). Within the Eastern terrane there are a few lenses of conodont-bearing marbles and paragneisses (Petrov and Borozdina 1996; Friberg and Petrov 1998), but their relationship to the Brodovo gneisses is not established. The gneisses are intruded by the Ermakov and East Emekh granites and the Basianovo gabbro (Sobolev et al. 1964).

Previous isotope studies of the Salda Metamorphic Complex

From 1968 to 1970, an extensive radiometric age determination program on gneiss complexes was carried out under the leadership of A.P. Grevtsova (unpublished data). Most of the work was done using the K–Ar method, mainly on whole-rock samples, but also on minerals. There are also a few multigrain Pb–Pb direct evaporation and conventional U–Pb determinations on zircons. The ages presented here (Table 1) have been recalculated using the standards adopted by IUGS subcommision on geochronology (Steiger and Jäger 1978).

The Pb–Pb work involved the analysis of populations of zircons from Teliana plagiogranites in the Western Terrane (samples A-3-3660 and A-L-46), yielding consistent ages of 345 and 340 Ma (Fig. 3; Table 1). In addition, two Pb–Pb ages were obtained from the Ermakov massif (Fig. 2) which yielded slightly different results. The plagiogranitic part in the core (sample A-L-14) yielded an age of 320 Ma (no error given) and the granite in the rim (sample A-KC-3741) 275 ± 25 Ma. A.P. Grevtsova et al. (unpublished data) presented 91 whole-rock K–Ar age determinations (Fig. 3; Table 1) including all the main lithologies in the Salda Metamorphic Complex; all but one show Paleozoic ages (260–590 Ma). Even though the accuracy of method can be questioned, the consistency of this large body of data suggests that all these rocks were formed and deformed in the Paleozoic. However, this was not accepted in the 1970s (high-grade metamorphic rocks were assumed to be old) and all the ages were inferred to reflect only the Paleozoic thermal overprint.

Table 1 Results of A.P. Grevtsova et al. (unpublished data). Ages have been recalculated using the decay constants given by Steiger and Jäger (1978). Coordinates refer to Fig. 2 and are given in kilometers. CL Central Laboratory at Urals Geological Survey, Ekaterineburg; IGG the Institute of Geology and Geochemistry, Ekaterineburg. n.d. not determined

Sample	Lithology	Age on	Method	Lab	X	Y	Age (Ma)
Central part of Gneiss domes							
2092	Granulite–amphibolite gneiss	Whole rock	K–Ar	CL	38.5	25	592 n.d.
1897	Amphibolite	Whole rock	K–Ar	CL	33.5	9	472 ± 37
1895	Amphibolite gneiss	Whole rock	K–Ar	CL	29	21	469 ± 15
1703	Granulite–amphibolite–biotite gneiss	Whole rock	K–Ar	CL	55.5	69	461 ± 7
2156	Biotie–amphibolite gneiss	Whole rock	K–Ar	CL	36	27	378 ± 35
2091	Amphibolite	Whole rock	K–Ar	CL	38	27	337 ± 30
2155	Amphibolite–biotite gneiss	Whole rock	K–Ar	CL	36	26	298 ± 28
2154	Amphibolite–biotite gneiss	Whole rock	K–Ar	CL	37	28.5	290 ± 13
Rim of Gneiss domes							
A-834	Amphibolite gneiss	Whole rock	K–Ar	IGG	57.5	34.5	399 n.d.
1685	Feldspar amphibolite	Whole rock	K–Ar	CL	41.5	42.5	396 ± 33
959	Biotite–amphibolite	Whole rock	K–Ar	CL	47.5	50.5	393 n.d.
1892	Quartz–muscovite schists	Whole rock	K–Ar	CL	57.5	32.5	387 ± 18
538	Amphibolite gneiss	Whole rock	K–Ar	CL			
1984	Granulite–biotite gneiss	Whole rock	K–Ar	CL	44.5	31	386 ± 12
1983	Granulite–two-mica gneiss	Whole rock	K–Ar	CL	44.5	31	373 n.d.
1702	Granulite–biotite–amphibolite gneiss	Whole rock	K–Ar	CL	57.5	70	368 ± 28
1771	Gneiss	Whole rock	K–Ar	CL	66.5	64	364 ± 12
963	Biotite–amphibolite gneiss	Whole rock	K–Ar	CL	47.5	50	363 ± 37
1019	Epidote–plagioclase amphibolite	Whole rock	K–Ar	CL	65	55.5	355 ± 31
1889	Two-mica gneiss	Whole rock	K–Ar	CL	55	35	348 ± 25
1899	Biotite gneiss	Whole rock	K–Ar	CL	55	35	339 ± 16
1211	Plagioclase amphibolite	Whole rock	K–Ar	CL	66.5	64	316 ± 2
1982	Granulite–biotite gneiss	Whole rock	K–Ar	CL	44.5	31	314 ± 6
1681	Gneiss	Whole rock	K–Ar	CL	42	32.5	345 n.d.
1715	Biotite–amphibolite gneiss	Whole rock	K–Ar	CL	47.5	49.5	314 ± 10
A-835	Gneiss	Whole rock	K–Ar	CL	55	35	288 n.d.
A-836	Gneiss	Biotite	K–Ar	CL	55	35	292 n.d.
Istok Mélange							
1679	Actinolite–chlorite schist	Whole rock	K–Ar	CL	50.5	29	431 ± 29
1714	Two-mica schist	Whole rock	K–Ar	CL	47	50	407 ± 11
960	Graphite–mica–quartz schist	Whole rock	K–Ar	CL	47	50	395 ± 1
1887	Epidote–mica schist	Whole rock	K–Ar	CL	53.5	12.5	392 ± 11
1707	Graphite–feldspar–micaschist	Whole rock	K–Ar	CL	45	50.5	387 ± 10
2093	Muscovite–quartzite	Whole rock	K–Ar	CL	51	17	378 ± 4
1743	Talc–carbonate–micaschist	Whole rock	K–Ar	CL	45	7.5	376 ± 24
1898	Graphite–mica–quartz schist	Whole rock	K–Ar	CL	45.5	30	374 ± 40
1712	Microamphibolite	Whole rock	K–Ar	CL	45.5	50.5	372 ± 6
A-833	Muscovite microgneiss	Muscovite	K–Ar	IGG	57.5	19.5	357 n.d.
1682	Two-mica microgneiss	Whole rock	K–Ar	CL	41	44.5	351 n.d.
1713	Biotite–quartz schist	Whole rock	K–Ar	CL	45	50.5	351 ± 36
1684	Muscovite–kyanite schist	Whole rock	K–Ar	CL	41	44.5	340 ± 4
1715	Schist?	Whole rock	K–Ar	CL	47.5	45.5	314 n.d.
1683	Amphibolite microgneiss	Whole rock	K–Ar	CL	42.5	41.5	309 ± 22
A-75-B	Mica schist	Biotite	K–Ar	IGG	51	15.5	307 n.d.
Istok Mélange							
1680	Mica–feldspar schist	Whole rock	K–Ar	CL	51	17	298 ± 3
1985	Feldspar–amphibolite schist	Whole rock	K–Ar	CL	63.5	29	285 ± 28
1686	Actinolite–biotite schist	Whole rock	K–Ar	CL	48.5	41.5	285 ± 11
1276	Amphibolite schist	Whole rock	K–Ar	CL	73	54.5	332 ± 2
1987	Quartz–muscovite–chlorite schist	Whole rock	K–Ar	CL	64.5	27	294 ± 14
1886	Chlorite schist	Whole rock	K–Ar	CL	63	19	269 ± 6
Well-preserved intrusive rocks							
1709	Gabbro–norite	Whole rock	K–Ar	CL	48.5	54.5	435 ± 34
1217	Amphibolite gabbro	Whole rock	K–Ar	CL	68	54.5	413 ± 10
964	Gabbro–amphibolite	Whole rock	K–Ar	CL	50	54	368 ± 14
1708	Gabbro–amphibolite	Whole rock	K–Ar	CL	51.5	53.5	367 ± 29
1013	Granodiorite	Whole rock	K–Ar	CL	28	79	410 ± 11
1016	Quartz diorite	Whole rock	K–Ar	CL	27.5	77.5	399 ± 7
545	Plagiogranite	Whole rock	K–Ar	CL	66.5	64	380 n.d.
589	Biotite plagiogranite	Whole rock	K–Ar	CL	*	*	374 ± 30
1215	Diorite	Muscovite	K–Ar	IGG	67.5	51	374 ± 26

For continuation of Table 1 please see next page

Table 1 Continued

Sample	Lithology	Age on	Method	Lab	X	Y	Age (Ma)
Well-preserved intrusive rocks							
1020	Diorite?	Whole rock	K–Ar	CL	66.5	50.5	425 n.d.
A-3–3660	Plagiogranite	Zircon, multigrain	Pb-Pb	IGG	25.5	56	345 ± 30
A-L-46	Plagiogranite	Zircon, multigrain	Pb-Pb	IGG	33	78	340 n.d.
A-L-14	Plagiogranite	Zircon, multigrain	Pb-Pb	IGG	28.5	75.5	320 n.d.
1008	Granite	Whole rock	K–Ar	CL	27.5	62.5	393 ± 17
1009	Granodiorite	Whole rock	K–Ar	CL	25	69	367 ± 8
567	Muscovite granite	Muscovite	K–Ar	CL	69	60.5	348 n.d.
1011	Granite	Whole rock	K–Ar	CL	38.5	61.5	338 n.d.
565	Granite	Whole rock	K–Ar	CL	66.5	57.5	312 n.d.
566	Two-mica granite	Whole rock	K–Ar	CL	63	55	312 n.d.
564	Biotite granite	Whole rock	K–Ar	CL	67.5	60	311 n.d.
540	Biotite granite	Whole rock	K–Ar	CL	*	*	300 ± 11
1010	Granite	Whole rock	K–Ar	CL	32	68	300 ± 4
958	Granite	Whole rock	K–Ar	CL	42.5	52	296 n.d.
1015	Granite	Whole rock	K–Ar	CL	38.5	56	278 ± 10
563	Biotite granite	Whole rock	K–Ar	CL	68.5	58.5	272 n.d.
A-KC-3741	Granite	Zircon, multigrain	Pb-Pb	IGG	26	68	275 ± 25
233	Porphyritic granite	Whole rock	K–Ar	CL	66.5	64	356 n.d.
230	Quartz–albite porphyry	Whole rock	K–Ar	CL	66.5	64	355 n.d.
1014	Andesite–dacite porphyry	Whole rock	K–Ar	CL	29.5	59.5	355 ± 1
Metasomatic rocks							
232	Epidote schist in skarn	Whole rock	K–Ar	CL	66.5	64	406 n.d.
1871	Preskarn quartz–feldspar	Whole rock	K–Ar	CL	*	*	394 n.d.
1/59.4	Epidote–chlorite-biotite skarn	Whole rock	K–Ar	CL	*	*	374 n.d.
1873	Post-skarn quartz–feldspar	Whole rock	K–Ar	CL*	*	360 n.d.	
1371	Plagio-gneiss greisen	Whole rock	K–Ar	CL	65.5	55.5	360 ± 11
546	Muscovite–gneiss greisen	Whole rock	K–Ar	CL	64.5	60.5	341 ± 9
Metasomatic rocks							
1939	Quartz–muscovite–biotite	Whole rock	K–Ar	CL	66.5	64	337 ± 15
1208	Muscovite greisen	Muscovite	K–Ar	CL	63.5	62	336 ± 6
1936	Mica greisen	Whole rock	K–Ar	CL	66.5	60.5	383 ± 11
1937	Greisen	Whole rock	K–Ar	CL	66.5	60.5	311 ± 23
1935	Greisen Zone	Microcline	K–Ar	CL	66.5	60.5	286 ± 15
Migmatites							
1872	Plagio-migmatite	Whole rock	K–Ar	CL	66.5	64	407 ± 5
1717	Plagio-migmatite	Feldspar	K–Ar	CL	66.5	64	318 ± 27
1711	Quartz–microcline–plagioclase	Whole rock	K–Ar	CL	46	54.5	315 n.d.
962	Aplite-like quartz feldspar rock	Whole rock	K–Ar	CL	*	*1033	313 ± 5
547	Biotite gneiss	Whole rock	K–Ar	CL	68	61	302 ± 7
1017	Two-mica granite-gneiss	Whole rock	K–Ar	CL	68	54.5	294 ± 18
1018	Granite/granitic gneiss	Whole rock	K–Ar	CL	68	62.5	269 ± 1
1209	Granite migmatite	Feldspar	K–Ar	CL	66.5	64	263 n.d.
Granite east of Salda Metamorphic Complex							
1212	Granite/granitic gneiss	Whole rock	K–Ar	CL	75.5	58.5	304 n.d.
1214	Granite/granitic gneiss	Whole rock	K–Ar	CL	75	53	416 n.d.
1218	Granite/granitic gneiss	Whole rock	K–Ar	CL	76	57.5	293 n.d.
1213	Granite/granitic gneiss	Whole rock	K–Ar	CL	83	53	313 n.d.
1021	Granite/granitic gneiss	Whole rock	K–Ar	CL	85	52.5	318 n.d.
Murzinka-Adui Metamorphic Complex (south of Fig. 3)							
K-29-1	Biotite gneiss	Zircon, multigrain	U–Pb	IGG	*	*	910 ± 60
1328	Biotite gneiss	Zircon, multigrain	U–Pb	IGG	*	*	470 ± 50
K-23-2	Biotite gneiss	Zircon, multigrain	U–Pb	IGG	*	*	465 ± 30
1300	Biotite gneiss	Zircon, multigrain	U–Pb	IGG	*	*	360 ± 40
2020	Biotite gneiss	Whole rock	K–Ar	CL	*	*	340 ± 13
1325	Gneiss	Zircon, multigrain	U–Pb	IGG	*	*	315 ± 30
2021	Biotite–sillimanite gneiss	Whole rock	K–Ar	CL	*	*	277 ± 23
1326	Amphibolite gneiss	Zircon, multigrain	U–Pb	IGG	*	*	260 ± 24
1299	Biotite gneiss	Zircon, multigrain	U–Pb	IGG	*	*	260 ± 24
916	Gneiss	Whole rock	K–Ar	IG	*	*	248 n.d.
2026	Granulite–biotite gneiss	Whole rock	K–Ar	CL	*	*	247 n.d.
2024	Biotite gneiss	Whole rock	K–Ar	CL	*	*	240 n.d.
948	Gneiss	Whole rock	K–Ar	IG	*	*	244 n.d.
2017	Biotite gneiss	Whole rock	K–Ar	CL	*	*	176 n.d.
2022	Two-mica gneiss	Whole rock	K–Ar	CL	*	*	174 n.d.

The only indication of older ages in the Salda Metamorphic Complex are strongly discordant U–Pb ages by Krasnobayev (1986) obtained on various lithologies from within or near the Prianitchnikova Shear Zone (location imprecise). The results spread evenly from 900 to 2200 Ma (no errors given). A sample of similar lithology has been re-examined (sample 71) in this work and no supporting evidence for the Precambrian ages has been obtained.

Description of samples

We collected representative rocks from the Salda Metamorphic Complex (Fig. 3), including some of the same lithologies that were sampled by previous workers (Krasnobayev 1986; A.P. Grevtsova et al., unpublished data) for comparison of results. In addition, we attempted to date metamorphic rocks, which occur east of the Salda Metamorphic Complex (samples 295 and 326), but the zircon populations proved inadequate and the results are preliminary. From the Western Terrane of the Salda Metamorphic Complex, we sampled both the Emekh mafic gneisses (sample 24) and the Teliana igneous suite, the latter including granodiorites at the type locality (sample 60) and granulite-facies gabbros (samples 71 and 69). We also sampled the Brodovo garnet-bearing mafic and felsic gneisses (samples 80, 268, 163 and 136) from the Eastern Terrane. In addition, samples were collected from the cross-cutting East Emekh granite (sample 147) and Basianovo gabbro (sample 32).

The sample of Emekh mafic gneiss (sample 24) consists of granulite-facies assemblages, including plagioclase, clinopyroxene, hornblende, garnet and minor, epidote, titanite, apatite and magnetite. Plagioclase–amphibole symplectites replace garnet and hornblende replaces pyroxene. A planar orientation of amphiboles defines the foliation. Peak metamorphism was approximately 800 °C based on garnet and clinopyroxene compositions (Petrov, in press).

The three Teliana suite samples include a granodiorite (sample 60) that is dominated by plagioclase and quartz, with subordinate biotite, epidote and minor hornblende. It has a weak upright foliation defined by aligned biotite. The second Teliana sample (sample 71) is a banded gneiss consisting of amphibole and clinopyroxene together with garnet. These samples have a clear prograde metamorphic path with temperature increasing from approximately 500 °C (hornblende plagioclase) to approximately 800 °C (garnet–clinopyroxene) and pressure from approximately 6 to approximately 10 kbar at peak metamorphism. The third Teliana sample (69) is less deformed, with ortho-, clinopyroxene and plagioclase together with secondary quartz and hornblende defining a pronounced foliation. This rock, of gabbroic composition, has kept many of its primary magmatic features. The metamorphic history only shows retrogression from granulite (ca. 850 °C clinopyroxene–orthopyroxene geothermometry) to amphibolite facies and nothing of the prograde metamorphism present in the surrounding rocks (Petrov et al. 1998; Petrov, in press).

Of the samples from the Brodovo orthogneisses of the Eastern Terrane, two (samples 268 and 136) were collected from within the Prianitchnikova Shear Zone; sample 268 contains hornblende, plagioclase and quartz, overgrown by garnet and clinopyroxene, and sample 136 is dominated by plagioclase, quartz and amphibole, with minor garnet ± biotite. Planar-oriented amphibole defines a strong penetrative foliation in these isoclinally folded gneisses. The intermediate component of the Brodovo gneisses (sample 80) carries garnet and is dominated by plagioclase and amphibole with minor biotite and quartz. It has a strong gneissic fabric and is dioritic in composition. Sample 163, also from the Brodovo gneisses, comes from the northern part of the area and is a fine-grained granodiorite gneiss with garnet and plagioclase porphyroblasts in a quartz, plagioclase and biotite matrix. All samples from the Brodovo gneisses show the same prograde metamorphic history (Petrov et al. 1998; Petrov, in press) from lower amphibolite facies (500 °C and 6 kbar) to upper amphibolite/granulite facies (700–800 °C and 8 kbar).

Gabbros from the Basianovo intrusion (sample 32) are dominated by plagioclase and clinopyroxene, the latter partly replaced by amphibole; subordinate minerals are biotite, apatite, titanite and magnetite. The amphiboles have a planar orientation and the plagioclases are granulated, giving the rock a gneissosity. Studies of geothermobarometry (Petrov, in press) indicate crystallization at shallow crustal levels (< 4 kbar). The East Emekh pluton (sample 147) is a coarse-grained, plagioclase, microcline, quartz, hornblende and biotite-bearing granite. It cuts the foliation in the host-rock Brodovo gneisses.

Analytical procedure

In this study the single zircon Pb-evaporation technique (Kober 1986, 1987), described by many authors (e.g. Hellman et al. 1997, and references therein; Dougherty-Page and Bartlett 1999), was applied.

Zircons were separated by standard methods at the Urals Geological Survey Expedition's laboratory. They were then hand-picked and analysed by one of us (A.L.) at the laboratory for Isotope Geology at the Swedish Museum of Natural History (NRM), using a Finnigan MAT 261 (Finnigan, Bremen, Germany) mass spectrometer. Each zircon to be analysed is placed into a "canoe"-shaped rhenium filament as part of a double filament assemblage, so that the slit of the "canoe" faces a flat ionization filament. Thereafter, the zircons are heated stepwise from approx-

imately 1450 to approximately 1600 °C (with increments of 10–30 °C per step, monitored by a pyrometer). During heating zircon breaks down to baddeleyite (Chapman and Roddick 1994), and the released lead is plated onto the adjacent ionization filament and analysed. Lead emission from the ionization filament was observed at approximately 1350–1400 °C. Data were collected in a peak-jumping mode using a secondary ion multiplier, with each scan encompassing the sequence 206Pb–207Pb–208Pb–206Pb–204Pb. The ion multiplier was regularly calibrated against the NBS 983 standard. For every heating step, one to three blocks of ten scans were registered. Extreme values were eliminated using the Dixon test (Dixon 1950). Correction for common lead was made using the measured $^{206}Pb/^{204}Pb$ ratio and the two-stage model proposed by Stacey and Kramers (1975). The calculations of the $^{207}Pb/^{206}Pb$ ages for each scan were done using software designed by T. Persson at the NRM and the age for each evaporation step was determined with the "Histogram" procedure of the "ISOPLOT" program (Ludwig 1991). For those grains where analyses at increasing temperature reached a "plateau age", i.e. higher temperature steps that show consistent ages. Ages and the corresponding errors were calculated for the sample by weighted averages based on the evaporation steps in the plateaus (Ludwig 1991). The lead emission from the zircons can drop significantly towards the end of the analyses yielding unreliable results. These steps were excluded from the age calculations. The evaporation steps excluded from the age calculations are marked with an asterisk in Table 2.

At young ages, close to 300 Ma, the influence of mass fractionation might be significant, and various methods to correct for this have been suggested. These are sometimes based on ad hoc assumptions or long-time monitoring of several analyses, repeated under similar conditions. It is, however, not possible in the single zircon evaporation method to measure the degree of mass fractionation in each separate analysis, and we therefore chose not to correct for it.

It has been shown by many studies (e.g. Kober et al. 1987; Kröner et al. 1988; Karabinos et al. 1989; Ansdell and Kyser 1991) that the plateau ages and, usually, the oldest and last evaporation steps correlate well in age with upper intercepts in conventional U–Pb zircon analyses; others, e.g. Cocherie et al. (1992), and Paquette et al. (1994), have found that this method can yield slightly younger ages than conventional U–Pb zircon analyses.

Zircon morphology

The zircons from the Emekh gneisses (sample 24) are clear, anhedral and somewhat brownish. Zircons from the different samples of the Teliana intrusive suite vary greatly in appearance. The granodiorite (sample 60) has clear zircons, some of which are slightly prismatic, but most are anhedral. They are commonly light brown under direct light and often contain apatite needles, indicative of a magmatic origin. The two mafic granulite samples (71 and 69) have similar zircon populations with both sub- and anhedral crystals. They are often broken and, even though some crystals are clear, the majority are full of small inclusions. Frequently, there is an inclusion-free core that is always much darker than the overgrowth.

The samples from the Eastern Terrane, e.g. the Brodovo intrusive suite (samples 80, 136, 163 and 268) display magmatic zonation and often have darker cores. The most well preserved are the crystals from the granodioritic granulites (sample 268). These grains are completely transparent, with igneous zoning and a thin metamorphic rim. The amphibolite-facies felsic gneisses (samples 80 and 136) have subhedral and darker zircons with many inclusions. The Brodovo felsic gneiss from further north in the Eastern Terrane (sample 163) has small subhedral zircons with a clear core and magmatic zonation, overgrown by a rim that often contains inclusions. These grains show signs of both resorption and overgrowth of their primary magmatic domains and can contain three generations of growth events.

In the Basianovo gabbro (sample 32), the zircons are very clear, contain many inclusions and often have radial cracks. Magmatic zonation is evident and the morphology is sometimes subhedral. The last sample is from the East Emekh pluton (sample 147). It has clear, prismatic zircons with pronounced magmatic zonation.

Results

Figure 5 and Table 2 present the data. Zircons from the Emekh mafic gneisses (24), Murzinka-Adui (sample 295) and Krasnogvardeiskii (sample 326) complexes contained so little radiogenic lead that the results obtained are to be considered as preliminary. Unfortunately, only one grain from the Brodovo intrusive suite in the northern part of the area (sample 163) was suitable for analysis.

Based on field relationships, we interpret the Emekh gneisses to be the oldest of the rocks exposed in the Salda Metamorphic Complex. The oldest grain (24d; Table 2) has a minimum crystallization age of approximately 500 Ma. There are no previous age determinations on these rocks.

The complex grains from the Brodovo intrusive suite, i.e. samples 80, 136 and 268, do not show any consistent plateaus but seem to have intricate core/overgrowth relations. We have chosen not to calculate any mean ages for the samples 80 and 136, only to present an interpretation of the data. Most of the ages from the Brodovo intrusive suite are in the range

Table 2 Results from the single zircon Pb/Pb evaporation analyses. Results marked with an asterisk are not included in the age calculations

Sample/step	Temp (°C)	Ratios	206/204 ± 2σ		207/206 ± σ		Age ± σ
Brodovo Intrusive Suite							
Sample 80. Intermediate gneiss. No mean age calculated							
80a6	1480	20	9400	9600	0.05638	73	299 ± 140*
80a7	1480	18	31000	23000	0.05575	76	394 ± 90
80a8	1520	20	13500	7300	0.05550	39	368 ± 39
80a9	1520	20	9900	2000	0.05456	46	322 ± 54
80a10	1550	20	17400	9600	0.05519	58	362 ± 40
80a11	1550	19	39000	26000	0.05425	43	368 ± 37
80a12	1550	20	25800	6900	0.05421	35	349 ± 36
80a13	1570	18	52000	23000	0.05430	56	362 ± 53
							Average 360 ± 55
80b3	1490	19	6890	970	0.05596	51	356 ± 64
80b4	1500	13	10200	3400	0.05552	73	354 ± 65
80b5	1500	17	39000	17000	0.05440	44	361 ± 42
80b6	1520	18	35000	26000	0.05517	63	368 ± 56
80b7	1540	10	21000	12000	0.05468	49	356 ± 33
80b8	1570	19	36000	19000	0.05482	37	381 ± 34
80b9	1570	20	8500	2200	0.05404	43	286 ± 44*
							Average 362 ± 51
80c3	1470	20	28000	23000	0.05421	49	306 ± 76*
80c4	1480	7	90000	140000	0.05486	67	379 ± 27
80c5	1500	14	93000	57000	0.05513	37	407 ± 29
80c6	1530	19	67000	86000	0.05466	44	370 ± 39
							Average 387 ± 37
80d3	1500	20	5000	1000	0.05765	40	376 ± 77
80d5	1500	20	4440	620	0.05876	41	422 ± 50
80d6	1520	20	19600	5600	0.05563	30	397 ± 29
80d7	1520	10	14000	11000	0.05860	240	435 ± 120
							Average 403 ± 71
80e5	1500	19	51000	14000	0.05514	39	402 ± 36
80e6	1520	14	28000	15000	0.05489	51	378 ± 36
80e7	1520	14	32000	10000	0.05432	41	353 ± 34
80e8	1540	10	8900	3700	0.05631	61	384 ± 42
							Average 376 ± 41
Sample 136. Felsic gneisses. No mean age calculated							
136a4	1500	9	2800	1400	0.05880	270	290 ± 160*
136a6	1550	8	29000	20000	0.05600	160	448 ± 72
136a7	1580	20	34000	26000	0.05616	42	410 ± 33
							Average 421 ± 49
136b3	1530	18	2210	480	0.06060	130	329 ± 150
136b4	1550	10	1570	250	0.06500	110	421 ± 88
136b5	1580	8	1670	320	0.06155	53	287 ± 130
							Average 363 ± 117
136c3	1460	10	9000	2700	0.05546	82	354 ± 53
136c4	1490	20	9200	5100	0.05694	46	395 ± 60
136c5	1500	20	4090	630	0.05890	53	410 ± 62
136c6	1500	10	3300	790	0.05970	68	404 ± 63
136c7	1530	20	2220	140	0.06148	58	403 ± 46
136c8	1540	20	2910	340	0.06060	130	420 ± 120
136c9	1570	20	4300	280	0.05996	30	472 ± 31
							No mean calculated
136d2	1480	20	3300	480	0.05882	76	366 ± 96
136d3	1520	20	4910	970	0.05813	72	396 ± 88
136d4	1560	20	9600	1800	0.05624	40	389 ± 49
136d6	1560	20	13100	9700	0.05746	63	430 ± 78
136d7	1580	8	21000	10000	0.05740	86	473 ± 30
							No mean calculated
136e1	1470	20	1510	120	0.06325	86	338 ± 87*
136e2	1470	20	6310	900	0.05671	47	379 ± 48
136e3	1490	20	4690	410	0.05773	59	391 ± 48
136e4	1500	20	2700	330	0.06053	53	401 ± 66
136e5	1540	20	5300	1400	0.05834	79	392 ± 62
136e6	1570	20	7100	1300	0.05708	34	401 ± 41
136e7	1580	20	7500	1200	0.05724	39	416 ± 36
							Average 397 ± 66

For continuation of Table 2 please see next page

Table 2 Continued

Sample/step	Temp (°C)	Ratios	206/204 ± 2σ		207/206 ± σ		Age ± σ
Sample 136. Felsic gneisses. No mean age calculated							
136f3	1500	20	2370	470	0.06049	67	345 ± 110*
136f4	1540	19	3940	500	0.05884	33	406 ± 62
136f5	1570	20	2450	310	0.06081	69	385 ± 110
							Average 390 ± 66
Sample 163. Felsic gneisses. No mean age calculated							
163a3	1470	10	25000	14000	0.05443	95	350 ± 67
163a4	1480	28	20400	6600	0.05457	39	348 ± 43
163a5	1500	29	37000	27000	0.05381	73	320 ± 80
163a6	1520	25	67000	53000	0.05471	33	370 ± 33
163a7	1570	28	72000	63000	0.05408	74	367 ± 36
163a8	1590	30	37000	14000	0.05398	32	342 ± 45
163a9	1600	18	32000	12000	0.05378	26	335 ± 20
163a10	1600	27	62000	33000	0.05391	30	345 ± 29
							Average 347 ± 48
Sample 268. Felsic gneisses. Weighted average 393 ± 5 (95 % conf.)							
268a2	1480	20	4000	400	0.05780	100	370 ± 87*
268a3	1490	20	2630	250	0.05850	120	314 ± 110*
268a4	1500	20	2340	190	0.06059	62	378 ± 37*
268a5	1510	20	2460	150	0.06089	27	406 ± 29
268a6	1520	20	2115	97	0.06224	28	423 ± 34
268a7	1550	19	1640	290	0.06510	230	400 ± 130
268a8	1550	20	2050	360	0.06290	150	401 ± 55
268a9	1570	20	1770	250	0.06350	130	392 ± 66
268a10	1580	20	1059	97	0.06960	260	413 ± 88
							Average 410 ± 62
268b2	1500	20	11700	1900	0.05562	22	382 ± 29
268b3	1500	10	5400	1000	0.05729	54	388 ± 42
268b4	1540	19	24000	25000	0.05575	36	392 ± 31
268b5	1560	20	10900	6100	0.05615	85	372 ± 78
							Average 383 ± 50
268c2	1500	5	26000	52000	0.05480	100	287 ± 70*
268c3	1510	20	71000	62000	0.05556	39	386 ± 74
268c4	1520	20	38000	11000	0.05486	37	384 ± 41
268c5	1540	4	70000	150000	0.05610	130	424 ± 17*
268c6	1570	19	25900	6300	0.05530	30	396 ± 30
268c7	1600	19	17800	5300	0.05566	75	400 ± 64
							Average 392 ± 55
268d1	1440	10	6300	4500	0.05745	48	377 ± 41
268d2	1460	20	16000	680	0.05528	12	386 ± 11
268d3	1480	19	24600	3200	0.05528	8	396 ± 11
268d4	1490	20	17700	1800	0.05488	15	371 ± 16
268d5	1500	20	20500	2300	0.05550	14	402 ± 16
268d7	1520	20	5360	540	0.05560	130	339 ± 62
268d8	1540	12	11400	1200	0.05596	77	397 ± 51
268d9	1540	19	10500	1400	0.05594	32	389 ± 21
268d10	1550	17	12200	1800	0.05591	23	396 ± 14
							Average 383 ± 36
268e3	1500	5	2110	400	0.05950	100	333 ± 39*
268e4	1530	20	1972	66	0.06258	30	417 ± 40
268e5	1540	20	3380	180	0.05978	26	429 ± 29
268e6	1540	15	4940	480	0.05778	28	401 ± 30
268e7	1540	9	9000	11000	0.05901	66	438 ± 57
268e8	1570	17	8000	1200	0.05671	26	400 ± 37
268e9	1600	10	10900	3400	0.05514	35	381 ± 37
							Average 403 ± 47
Emekh gneisses							
Sample 24. Mafic gneiss. No mean age calculated							
24a3	1490	9	2280	360	0.05919	51	308 ± 68
24a4	1520	9	2600	1300	0.05940	140	280 ± 130
							No mean calculated
24b3	1520	8	624	45	0.08026	70	481 ± 72
24c3	1520	11	532	69	0.07810	140	290 ± 160
24d1	1480	15	286	18	0.1091	29	508 ± 170
24d2	1520	18	2290	950	0.0666	16	527 ± 150
							No mean calculated

For continuation of Table 2 please see next page

Table 2 Continued

Sample/step	Temp (°C)	Ratios	206/204 ± 2σ		207/206 ± σ		Age ± σ
Teliana Intrusive Suite							
Sample 60. Granodiorite. Weighted average 359 ± 5 (95 % conf.)							
60a4	1510	10	17600	7900	0.05430	100	337 ± 60*
60a6	1530	10	1789	440	0.05634	68	50 ± 190*
60a7	1550	30	16900	4100	0.05471	15	354 ± 30
60a8	1550	10	6200	1300	0.05580	14	337 ± 91
							Average 350 ± 51
60b3	1470	30	30200	7600	0.05441	18	363 ± 20
60b4	1490	30	23900	6100	0.05448	54	344 ± 71
60b6	1550	20	42000	23000	0.05452	30	360 ± 27
60b7	1560	16	51000	30000	0.05459	27	374 ± 26
60b8	1600	24	54000	19000	0.05430	24	366 ± 20
							Average 360 ± 42
60c2	1480	9	6900	4500	0.05890	100	417 ± 91
60c4	1540	30	17200	7600	0.05500	24	360 ± 33
60c5	1540	30	9600	1100	0.05601	28	383 ± 38
60c6	1570	10	4300	2100	0.05923	60	407 ± 86
							Average 381 ± 55
60d6	1550	10	4260	840	0.05853	73	407 ± 60
60d7	1580	27	18000	16000	0.05578	43	361 ± 61
							Average 373 ± 64
60e1	1460	20	10000	4800	0.05568	67	316 ± 36*
60e2	1480	20	31000	26000	0.05478	17	366 ± 19
60e5	1500	12	12400	1400	0.05468	32	348 ± 24
							Average 359 ± 22
60f1	1460	20	8700	1900	0.05481	80	319 ± 73
60f2	1480	20	25200	4700	0.05434	41	357 ± 43
60f3	1490	20	24700	5600	0.05429	18	354 ± 22
60f4	1500	20	20100	3200	0.05431	15	350 ± 19
60f5	1510	20	28500	6700	0.05441	20	362 ± 23
60f6	1540	17	22100	2500	0.05434	13	356 ± 11
60f7	1550	20	20600	2600	0.05450	20	360 ± 22
60f8	1580	20	20100	5100	0.05446	23	352 ± 24
							Average 351 ± 37
60g2	1490	17	31000	13000	0.05467	85	362 ± 69
60g3	1500	19	27000	10000	0.05516	73	381 ± 74
60g4	1520	18	80000	110000	0.05440	89	354 ± 81
60g5	1530	17	4750	660	0.05656	24	342 ± 27
60g6	1550	20	3420	270	0.05817	25	361 ± 46
60g7	1570	20	6470	660	0.05624	34	366 ± 30
							Average 362 ± 58
Sample 69. Granulite gabbro. Weighted average from all grains 361 ± 10 (95 % conf.). Weighted average excluding grain 69f 357 ± 7 (95 % conf.)							
69b2	1480	10	13000	17000	0.05600	180	335 ± 110
69b3	1500	14	11700	8500	0.05584	54	369 ± 47
69b4	1520	19	17300	7300	0.05482	20	355 ± 26
69b5	1520	16	15800	3100	0.05495	26	366 ± 29
69b6	1530	20	14300	4100	0.05481	35	354 ± 29
69b7	1560	20	4160	280	0.05725	56	366 ± 23
69b8	1600	10	9600	3300	0.05553	80	361 ± 56
							Average 362 ± 37
69c2	1500	20	6100	420	0.05550	110	351 ± 23
69c3	1520	19	7380	710	0.05561	13	352 ± 20
69c4	1540	20	10400	2100	0.05534	37	360 ± 30
							Average 355 ± 25
69d3	1520	20	14600	5600	0.05519	54	360 ± 54
69d5	1560	14	18400	7900	0.05654	48	417 ± 61
							Average 384 ± 63
69e1	1460	19	8800	1800	0.05576	15	367 ± 27
69e2	1470	20	7400	390	0.05553	13	352 ± 13
69e3	1500	20	6800	520	0.05588	26	357 ± 25
69e4	1520	20	4080	570	0.05534	61	316 ± 33*
							Average 359 ± 23
69f2	1480	20	16400	4800	0.05581	75	394 ± 68
69f3	1500	20	39000	42000	0.05624	41	428 ± 32
69f4	1500	14	23000	11000	0.05650	81	436 ± 66
							Average 418 ± 59

For continuation of Table 2 please see next page

Table 2 Continued

Sample/step	Temp (°C)	Ratios	206/204 ± 2σ		207/206 ± σ		Age ± σ
Sample 71. Mafic gneiss. Weighted average 343 ± 9 (95 % conf.)							
71a2	1460	10	4600	1700	0.05519	97	252 ± 81*
71a3	1500	13	6100	1600	0.05576	60	328 ± 61
71a4	1540	13	7700	1200	0.05578	29	360 ± 21
71a5	1580	16	9750	770	0.05500	24	348 ± 21
							Average 346 ± 39
71b1	1460	20	8400	1600	0.05510	55	339 ± 35
71b2	1500	20	13800	1400	0.05404	11	326 ± 16
							Average 330 ± 24
71c3	1460	10	6000	2000	0.05653	94	356 ± 42
71c4	1500	16	5300	1300	0.05644	88	336 ± 64
71c5	1520	10	17000	23000	0.05610	100	326 ± 81
71c6	1540	7	6300	2000	0.05595	63	348 ± 39
71c7	1570	7	2390	460	0.06101	65	376 ± 95
							Average 348 ± 64
71d1	1460	18	4690	440	0.05677	46	352 ± 35
71d2	1480	10	6090	790	0.05600	54	351 ± 31
							Average 352 ± 33
Cross-cutting intrusions							
Sample 32. Basianovo gabbro. Weighted average 336 ± 2 (95 % conf.)							
32a2	1440	5	15200	5800	0.05440	180	342 ± 55
32a3	1480	17	136000	84000	0.05314	31	324 ± 30
32a4	1480	12	111000	99000	0.05307	48	315 ± 29
32a5	1480	30	41000	20000	0.05317	28	301 ± 43
32a6	1490	26	105000	63000	0.05295	63	330 ± 21
32a7	1500	10	24700	6800	0.05397	67	341 ± 45
32a8	1530	18	74000	71000	0.05438	37	357 ± 40
32a9	1550	24	128000	82000	0.05328	17	333 ± 18
32a10	1570	27	79000	34000	0.05318	19	321 ± 25
							Average 326 ± 36
32b2	1480	30	44000	15000	0.05387	26	344 ± 31
32b4	1500	16	24200	6100	0.05394	33	338 ± 30
32b5	1530	30	50000	30000	0.05395	26	342 ± 37
32b6	1570	29	35900	8900	0.05368	23	335 ± 34
							Average 340 ± 33
32d1	1570	19	1470	110	0.06254	88	301 ± 31*
32d2	1450	10	40500	2900	0.05360	10	339 ± 6
32d3	1470	20	48900	8100	0.05333	5	328 ± 7
32d4	1480	20	43500	3600	0.05352	7	336 ± 6
32d5	1500	20	56200	5600	0.05350	5	339 ± 5
32d6	1510	20	15700	1000	0.05411	7	336 ± 7
32d7	1540	10	12600	1000	0.05421	9	330 ± 9
							Average 335 ± 8
32f2	1460	14	105000	53000	0.05333	45	329 ± 37
32f3	1480	19	86000	67000	0.05380	24	348 ± 19
32f4	1500	20	9470	980	0.05508	14	349 ± 17
32f5	1500	17	79000	20000	0.05344	16	337 ± 14
32f6	1500	18	118000	59000	0.05364	16	347 ± 11
32f7	1500	12	37000	20000	0.05385	43	338 ± 29
							Average 342 ± 36
Sample 147. East Emekh granite. Weighted average 334 ± 4 (95 % conf.)							
147a2	1460	18	13400	3000	0.05459	28	343 ± 27
147a3	1470	10	32000	12000	0.05359	29	331 ± 10
147a5	1500	20	60000	23000	0.05363	14	341 ± 11
							Average 340 ± 19
147b1	1450	20	5980	530	0.05532	16	319 ± 26
147b2	1460	20	20700	2200	0.05389	12	336 ± 8
147b3	1460	20	37100	4800	0.05335	60	325 ± 58
147b4	1480	20	39300	4600	0.05364	11	339 ± 11
147b5	1490	20	14000	3400	0.05382	15	303 ± 28
147b6	1500	20	33400	3300	0.05343	12	328 ± 11
147b7	1540	10	52000	12000	0.05344	17	334 ± 12
							Average 325 ± 30
147c2	1470	20	8400	660	0.05479	20	329 ± 18
147c3	1480	20	9420	380	0.05486	12	341 ± 13
							Average 335 ± 17

For continuation of Table 2 please see next page

Table 2 Continued

Sample/step	Temp (°C)	Ratios	206/204 ± 2σ		207/206 ± σ		Age ± σ
Sample 147. East Emekh granite. Weighted average 334 ± 4 (95 % conf.)							
147d1	1440	20	3380	280	0.05746	43	328 ± 55
147d2	1450	20	27400	3600	0.05324	36	314 ± 36
147d3	1470	20	27300	7400	0.05351	56	321 ± 57
147d4	1480	20	44200	8200	0.05379	22	346 ± 21
147d5	1500	10	22900	6700	0.05349	35	316 ± 29
							Average 326 ± 45
Samples from other gneiss complexes							
Sample 295. Murzinka-Adui Met. Complex. Weighted average 372 ± 9							
295a1	1430	17	4180	330	0.05754	34	370 ± 21
295a2	1460	20	63000	26000	0.05414	34	362 ± 28
295a3	1480	20	73000	35000	0.05400	31	358 ± 29
295a4	1500	18	30000	11000	0.05476	29	377 ± 26
295a5		20	28800	8100	0.05464	27	372 ± 19
							Average 367 ± 25
295b1	1480	4	34000	47000	0.05470	160	372 ± 51
295b2	1480	13	10300	1700	0.05523	56	359 ± 27
295b3	1480	10	46000	16000	0.05511	32	400 ± 24
							Average 378 ± 35
Sample 326. Krasnogvardeiskii Metamorphic Complex. No mean age calculated							
326a1	1470	20	32700	2600	0.08240	43	1230 ± 230
326a2	1480	9	24500	23000	0.05606	68	439 ± 15
							No mean calculated
326c1	1480	10	16000	17000	0.05673	59	414 ± 40
326e1	1430	20	198	2.5	0.12777	38	358 ± 89
326e2	1460	20	4490	240	0.05471	14	259 ± 23
326e3	1480	18	4500	2200	0.05611	30	278 ± 47
							No mean calculated

360–420 Ma and we find it likely that this is the age of the intrusives, as the main domains in these zircons display magmatic zoning. After rejection of some evaporation steps at low temperature or low statistics, it is possible to estimate a precise age of 393 ± 5 Ma for sample 268. The older ages, obtained from the later evaporation steps in the Brodovo samples, are likely to be from the innermost cores which we interpret to be xenocrysts derived from the source rock of the magma (cf. Hawkins et al. 1996). This is evident in grain c in sample 136 (minimum ages of the older zircons are obtained at 472 ± 31 and 473 ± 30 Ma), but is also visible in samples 268 and 80 (Fig. 5; Table 2). Most grains show systematically older ages with increasing evaporation step and it is not possible to separate different growth events.

The granodiorite and two pyroxene mafic granulites from the Teliana igneous suite (samples 60 and 69, respectively) show consistent ages at 359 ± 5 and 357 ± 7 Ma and a less complex growth history than the Brodovo gneisses. A.P. Grevtsova et al. (unpublished data) obtained a 345 ± 30 Ma Pb–Pb multigrain age for the the same granodiorite further to the north. Grain 69f is significantly older, 417 ± 21 Ma (Fig. 5), than the other four grains from this sample, even though it has the same morphology as the other grains. This intrusion contains frequent ultra mafic xenoliths which could be derived from either the Emekh or the Brodovo gneisses, and it is possible that grain 69f is an xenocryst from one of these; it is therefore excluded from the age calculation. The strongly deformed mafic gneiss from within the Prianitchnikova Shear Zone, sample 71 has an ill-defined age at approximately 343 ± 9 Ma. Chemistry, mineralogy (Petrov et al. 1998) and zircon morphology is similar to the two less deformed samples from the Teliana suite. It is not possible from the data to tell if the difference in age between this sample and the other two samples in the Teliana igneous suite (60 and 69) is due to the later age intrusion, metamorphic overprint or imprecise analysis. The multigrain Pb–Pb direct evaporation age of approximately 340 Ma from similar high-grade gneisses further north indicates that the ages are consistent throughout this suite.

The Basianovo gabbro (sample 32) and the East Emekh granite (sample 147) yield well-defined ages of 336 ± 2 and 334 ± 4 Ma, respectively (Fig. 5), implying that they were generated during the same Early Carboniferous event. The Pb–Pb multigrain direct evaporation ages obtained by A.P. Grevtsova et al. (unpublished data) for the Ermakov pluton (i.e. ca. 320 Ma) are 10–20 Ma older than the Rb–Sr and

Fig. 5 Results from analyses. Plots show evaporation step vs age. Vertical lines indicate the standard deviation for each evaporation step. The histograms display age in 10-Ma intervals vs number of scans

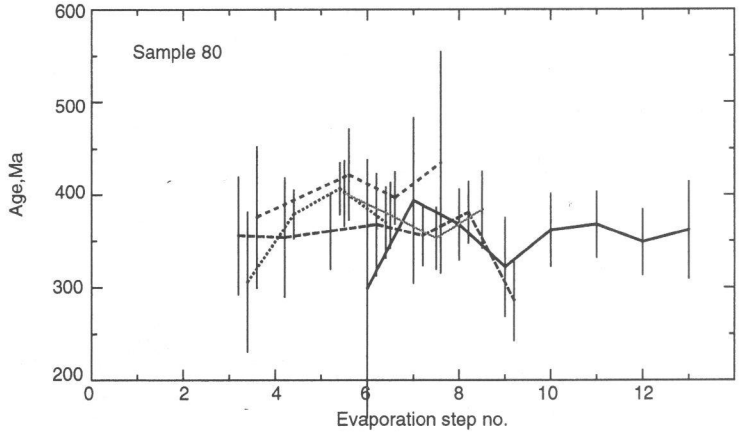
Sample 80
Age,Ma
Evaporation step no.

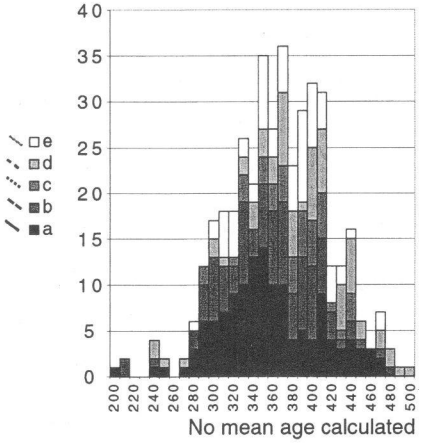
a
b
c
d
e
No mean age calculated

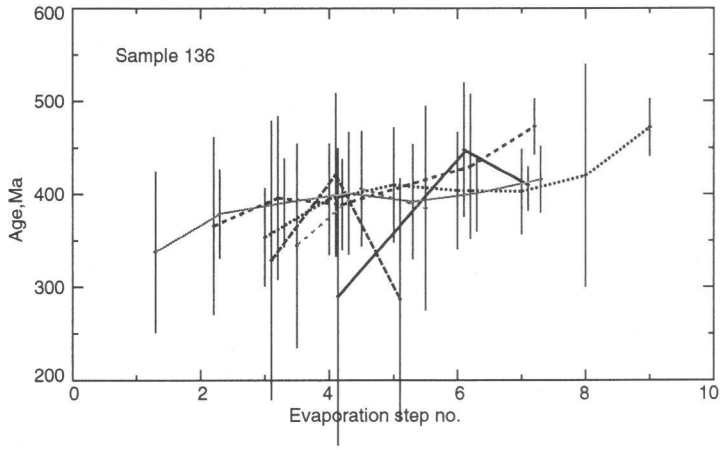
Sample 136
Age,Ma
Evaporation step no.

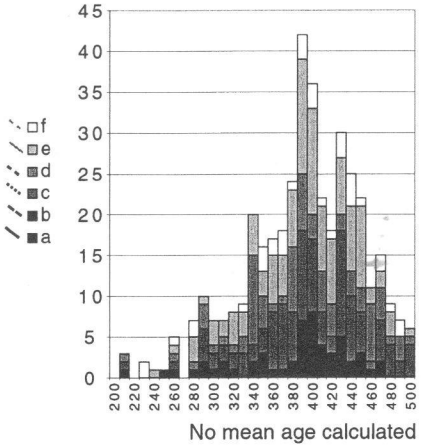
a
b
c
d
e
f
No mean age calculated

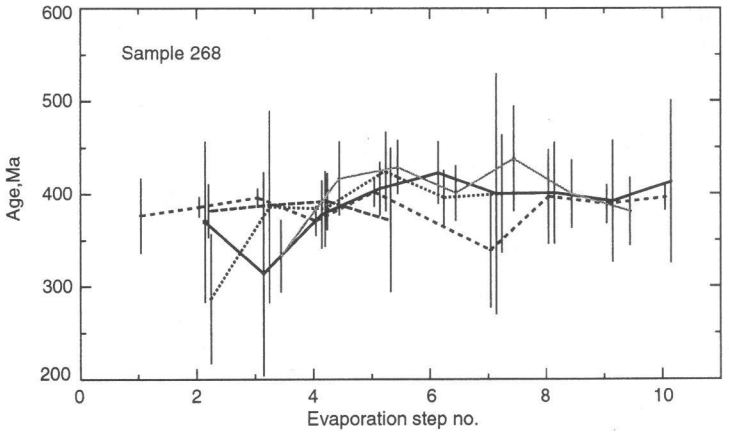
Sample 268
Age,Ma
Evaporation step no.

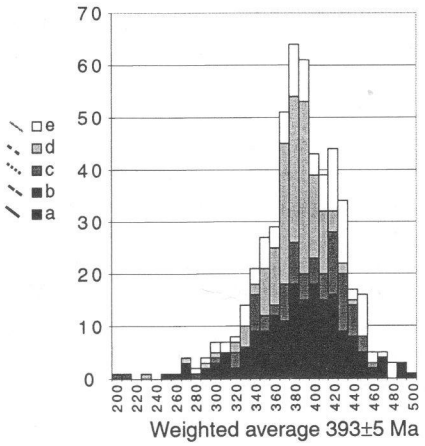
a
b
c
d
e
Weighted average 393±5 Ma

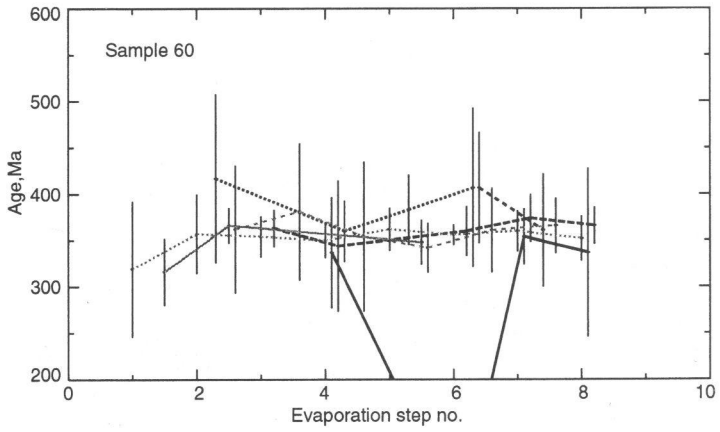
Sample 60
Age,Ma
Evaporation step no.

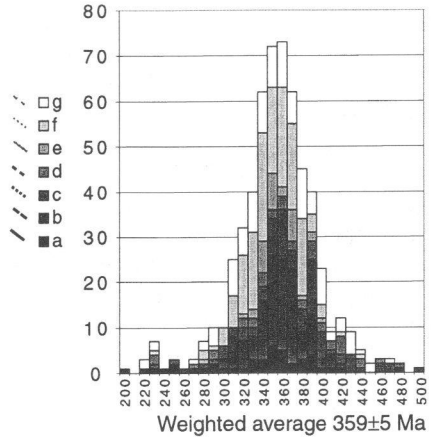
a
b
c
d
e
f
g
Weighted average 359±5 Ma

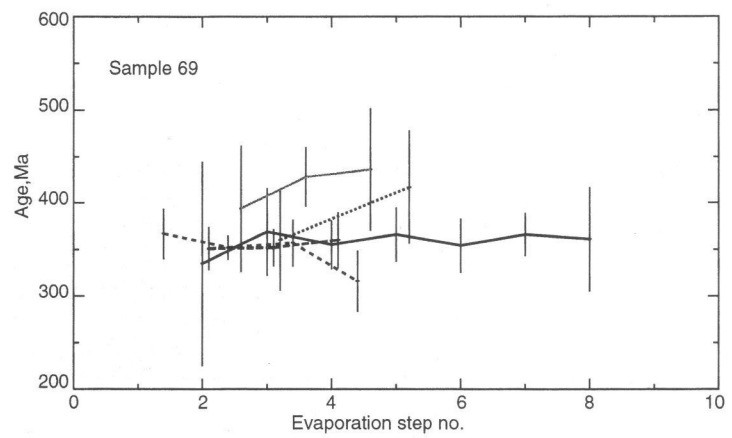
Sample 69
Age,Ma
Evaporation step no.

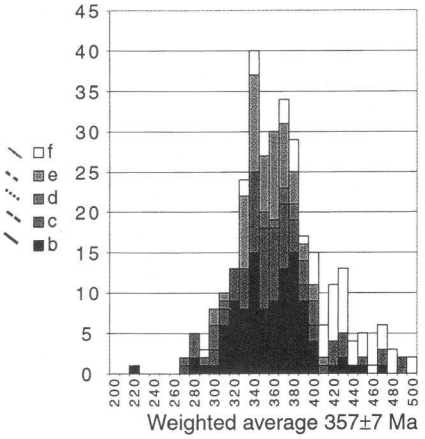
f
e
d
c
b
Weighted average 357±7 Ma

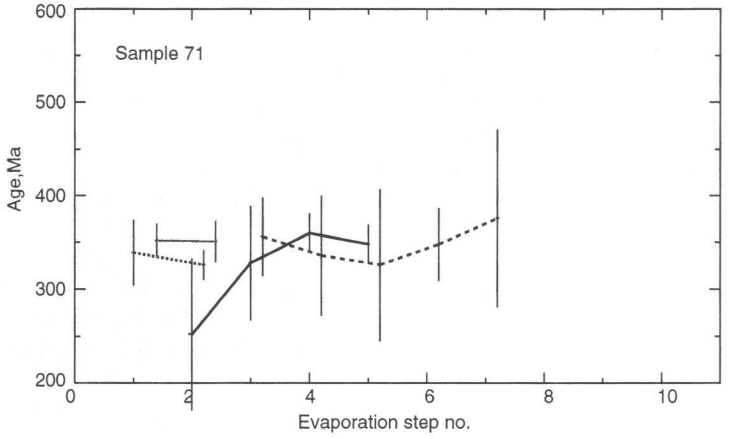
Sample 71
Age,Ma
Evaporation step no.

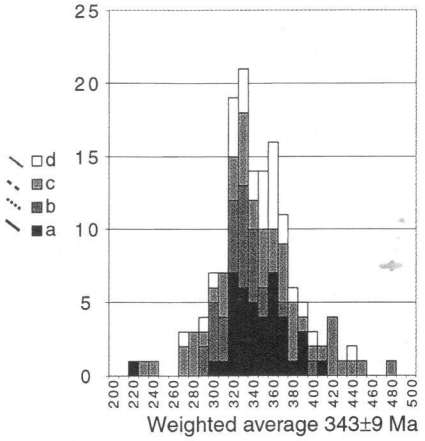
d
c
b
a
Weighted average 343±9 Ma

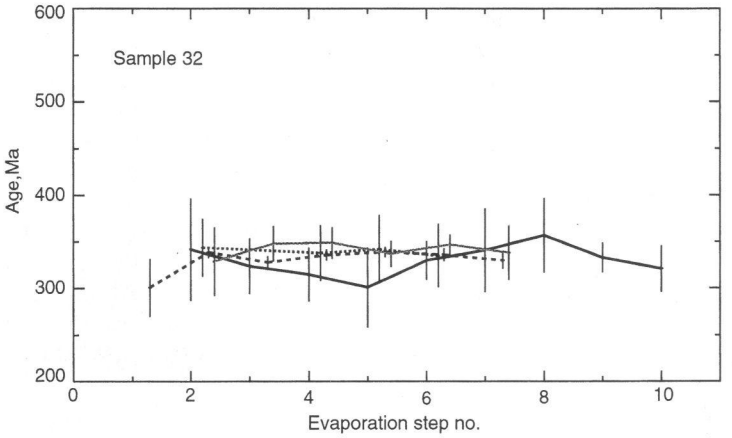
Sample 32
Age,Ma
Evaporation step no.

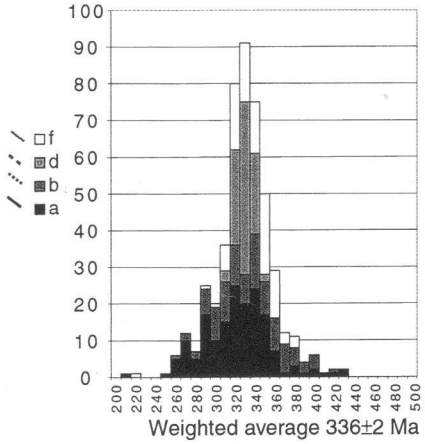
f
d
b
a
Weighted average 336±2 Ma

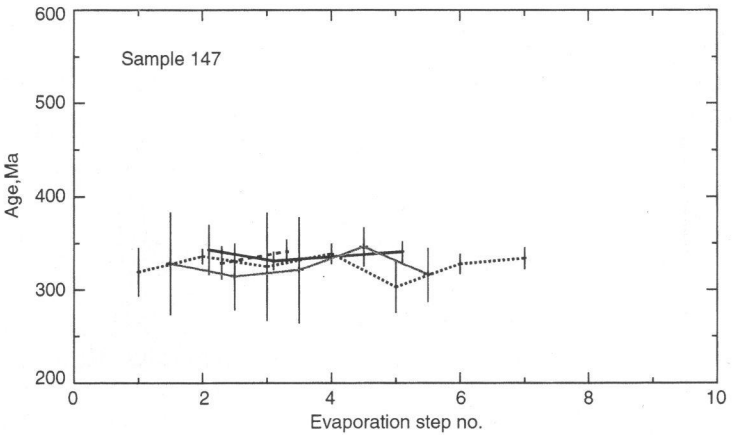
Sample 147
Age,Ma
Evaporation step no.

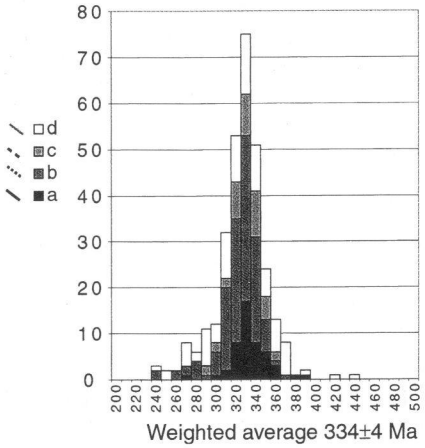
d
c
b
a
Weighted average 334±4 Ma

Sm–Nd ages obtained by Bea et al. (1997) for similar rocks further south. This may imply a northwards migration of magmatism with time or reflect the differences in closing temperatures. It can also be due to discrepancies between the analytical methods. The granitoids related to the migmatites probably have similar ages to those in the Verkhisetsk area; A.P. Grevtsova et al. (unpublished data) obtained ages near 280 Ma for the rim of the Ermakov massif, using whole-rock K–Ar and multigrain Pb–Pb direct evaporation methods.

In addition to the data presented above, we analysed two samples of metamorphic rocks from inliers southeast of the Salda Metamorphic Complex. The zircons from both of these are small and the majority are broken. Sample 326 comes from granitic gneisses of the Krasnogvardeiskii Metamorphic Complex. No plateau ages were obtained for any of the three zircons analysed from this sample. The grains 326a and 326b yield predominantly Devonian ages, whereas grain c indicates a Late Carboniferous event. The second sample (sample 295) was taken in the village of Biosovo (75 km north of Ekaterineburg) and is from the felsic part of banded mafic and felsic gneisses belonging to the Murzinka-Adui Metamorphic Complex. Only one of four grains yielded a well-defined plateau, 372 ± 9 Ma (Table 2); however, all data show Devonian ages. This is comparable with the results by A.P. Grevtsova et al. (unpublished data). None of the data provide evidence of Precambrian protoliths.

Discussion and conclusion

Most of the zircons analysed in this work contain only small amounts of radiogenic lead; thus, the 206Pb/208Pb and 206Pb/204Pb ratios are small (Table 2) and the precision is low. We therefore, for the interpretation of the data, assume that the errors are of the order of ±20 Ma, even if the calculated analytical errors are smaller.

Previous interpretations that the Salda Metamorphic Complex, together with the similar Murzinka-Adui, Krasnogvardeiskii and Sisert complexes, consist of old continental crust find no support in the new data. In the early plate tectonic interpretations, these terranes were thought to be old micro-continents that were accreted to the Siberian continent prior to the collision with Baltica (e.g. Potanin 1982; Zonenshain et al. 1984). Echtler et al. (1997) showed that this was not the case for the Sisert Complex. Work by A.P. Grevtsova et al. (unpublished data), presented in this paper provided little support for the existence of old, pre-Paleozoic, crust in the Murzinka-Adui and the Salda complexes. Our work has not eliminated the possibility of Precambrian crust being represented in the outboard terranes; however, the oldest zircons are of Ordovician age, and if Proterozoic rocks are present they must be very subordinate.

This study demonstrates that the Salda Metamorphic Complex started to form in the Late Silurian or Early Devonian when the igneous protoliths of the Brodovo orthogneisses (one sample indicate an age of 393 ± 5 Ma) intruded into some unknown host rock (= 470 Ma). Geochemical data from the Brodovo and Teliana igneous suites (Petrov 1995; Petrov et al. 1998) shows that these were subduction related, most probably originating in an intra-oceanic setting. The Emekh gneisses are derived from oceanic crust, probably as old as Cambrian and are cut by the Teliana intrusive suite (359 ± 5 and 357 ± 9 Ma) at deep crustal levels. The Western Terrane of the Salda Metamorphic Complex was thrust onto the Eastern Terrane sometime in the Early Carboniferous and this was followed by uplift and a third magmatic event that generated the bimodal magmas of the Basianovo gabbro and East-Emekh granite intrusions and perhaps also the Ermakov granite pluton: the last of these, dated to 334 ± 4 Ma, cuts the boundary between the two terranes, i.e. the Prianitchnikova Shear Zone.

The similarities in age and tectonic setting (i.e. Late Silurian to Early Devonian island arc) between Petrokamensk extrusive rocks and the Brodovo intrusive suite suggest that these are related. We interpret the metamorphosed Brodovo suite to be derived from the deep magmatic root of the Petrokamensk Volcanic Arc Complex. These volcanics resemble the Devonian Magnitogorsk volcanic arc in the Southern Urals and it is likely that this arc extends into the East Uralian Zone of the Middle Urals, lying to the east of the older Tagil Volcanic Arc Complex. Extrusive rocks related to the Early Carboniferous Teliana intrusive suite have not been recognized. It is possible that these intrusions were emplaced in the base of the pre-existing Petrokamensk Volcanic Arc Complex and were brought to the surface by thrusting along the Prianitchnikova Shear Zone. This interpretation is also supported by the fact that the highest-grade rocks are present between the Prianitchnikova thrust and neighboring normal fault (Fig. 3) and the two-pyroxene granulite gabbro only displays retrograde metamorphism.

The Salda Metamorphic Complex was uplifted from depths of approximately 30 to approximately 10 km before the emplacement of the Middle Carboniferous, East Emekh and Ermakov granites and Basianovo gabbro. The latter occurred during the development of the foreland basin, west of the Main Uralian Fault, i.e. while collision between Baltica and the island-arc terranes was still occurring. Much of uplift of the Salda Metamorphic Complex was probably along the thrust separating the Salda and Murzinka-Adui metamorphic complexes (Fig. 3), in combination with normal displacement on the Serov-Mauk and Prianitchnikova shear zones. The Permian granitoids identified throughout the East Uralian Zone (Bea at al. 1997; Fershtater et al. 1997) were emplaced at similar crustal levels as the Middle Carboniferous intrusions, implying that there was little uplift in the hinterland during the

development of the foreland fold-and-thrust belt. The final extension and uplift of the metamorphic rocks are likely to be coincident with the formation of the Triassic West Siberian Basin and related basins in the hinterland of the Middle Urals.

Acknowledgements Our thanks to the Saldinskaya Field Crew at the Urals Geological Survey Expedition for their support. Without them, this work would never have been accomplished. The thorough reviews by. A. Cocherie and F. Bea are greatly appreciated. We also thank INTAS for supporting co-operation between eastern and western scientists in the Urals. The field and laboratory work were financed by the Swedish Royal Academy of Science and Uppsala University. The work was conducted within the EUROPROBE Uralide project.

References

Ansdell KM, Kyser TK (1991) Plutonism, deformation, and metamorphism in the Proterozoic Flin Flon greenstone belt, Canada; limits on timing provided by the single-zircon Pb-evaporation technique. Geology 19:518–521

Antsigin NI et al. (eds) (1994) Descriptions of the stratigraphic schemes of the Urals. Urals Stratigraphic Committee, Ekaterinburg (in Russian)

Bea F, Fershtater G, Montero P, Smirnov V, Zin'kova E (1997) Generation and evolution of subduction-related batholiths from the central Urals: constraints on the P–T history of the Uralian orogen. Tectonophysics 276:103–116

Chapman HJ, Roddick JC (1994) Kinetics of Pb release during the zircon evaporation technique. Earth Planet Sci Lett 121:601–611

Cocherie A, Guerrot C, Rossi P (1992) Single-zircon dating by step-wise Pb evaporation; comparison with other geochronological techniques applied to the Hercynian granites of Corsica, France. Chem Geol 101:131–141

Dixon WJ (1950) Analysis of extreme values. Ann Math Stat 21:488–506

Dougherty-Page JS, Bartlett JM (1999) New analytical procedures to increase the resolution of zircon geochronology by the evaporation technique. Chem Geol 153:227–240

Echtler HP, Stiller M, Steinhoff F, Krawczyk C, Suleimanov A, Spiridonov V, Knapp JH, Menshikov Y, Alvarez-Marrón J, Yunusov N (1997) The tectono-metamorphic evolution of gneiss complexes in the Middle Urals, Russia: a reappraisal. Tectonophysics 276:229–251

Fershtater GB (1993) Magmatism and zonation of structural associations in the Urals. Geotectonics 26:435–444

Fershtater GB, Montero P, Borodina NS, Pushkarev EV, Smirnov V, Zin'kova E, Bea F (1997) Uralian magmatism: an overview. Tectonophysics 276:87–102

Friberg M, Petrov GA (1998) Tectonics of the Middle Urals: upper crustal structure east of the Main Uralian Fault. Geol J 33:37–48

Friberg M, Larionov A, Petrov GA, Gee DG (1997) Formation of juvenile continental crust in the hinterland of the Middle Urals during the Paleozoic orogeny. Terra Nova 9:1–118

Grevtsova AP, Zukozurnikova GA, Dolgal AS (1970) Isotopic age determinations of the Taratash and Salda Metamorphic complexes. USSR ministry of of Geology, Uralian Geological Board, Central Laboratory, Sverdlovsk (in Russian) (unpublished data)

Hamilton W (1970) The Uralides and the motion of the Russian and Siberian platforms. Geol Soc Am Bull 81:2553–2576

Hawkins DP, Bowring SA, Bradley IR, Karlstrom K, Williams ML (1996) U–Pb geochronologic constraints on the Paleoproterozoic crustal evolution of the Upper Granite Gorge, Grand Canyon, Arizona. Geol Soc Am Bull 108:1167–1181

Hellman FJ, Gee DG, Johansson Å, Witt-Nilsson P (1997) Single-zircon Pb evaporation geochronology constrains basement-cover relationships in the Lower Hecla Hoek Complex of northern Ny Friesland, Svalbard. Geochem Geol 137:117–134

Ivanov SN, Perfilyev AS, Yefimov AA, Smirnov GA, Necheukhin VM, Fershtater GB (1975) Fundamental features in the structure and evolution of the Urals. Am J Sci 275:107–130

Juhlin C, Gee DG, Kashubin S, Rybalka A, Hismatulin T (1993) Deep seismic reflection near the SG4 borehole, central Urals. Geol Föreningens Förhandl 115:315–320

Juhlin C, Friberg M, Echtler HP, Green AG, Ansorge J, Hismatulin T, Rybalka A (1998) Crustal structure of the Middle Urals: results from the ESRU experiments. Tectonics 17:710–725

Karabinos P, Kober B, Gromet LP (1989) Applications of single-grain zircon evaporation analyses; age discrimination in igneous suites and detrital grain studies. Geol Soc Am 21:268

Keilman GA (1974) Migmatite complexes of orogenic belts. Nedra, Moscow (in Russian)

Kober B (1986) Whole-grain evaporation for (super 207) Pb/(super 206) Pb-age investigations on single zircons using a double-filament thermal ion source. Contrib Mineral Petrol 93:482–490

Kober B (1987) Single-zircon evaporation combined with Pb+ emitter bedding for 207Pb/ 206Pb-age investigations using thermal ion mass spectrometry, and implications to zirconology. Contrib Mineral Petrol 93:63–71

Kober B, Pidgeon RT, Lippolt HJ (1987) Western Australian zircons with ages >4 Ga confirmed by Pb evaporation studies on single zircons in a thermal ion mass spectrometer. Fortschr Mineral Beih 65:97

Krasnobayev AA (1986) Zircon as indicator of geological processes. Nauka, Moscow (in Russian)

Kröner A, Reischmann T, Todt W, Zimmer M, Pallister JS (1988) Age and tectonic environment of Panafrican island arc assemblage in the Arabian-Nubian Shield as deduced from geochemistry and single grain zircon dating. Geological Association of Canada, Mineralogical Association of Canada, Canadian Geophysical Union, Joint Annual Meeting 13, p A69

Ludwig KR (1991) ISOPLOT: a plotting and regression program for radiogenic isotope data, version 2.56, US Geol Surv Open-File Report:91–445

Paquette J-L, Nédélec A, Bernard M, Rakotondrazafy (1994) U–Pb, single zircon evaporation, and Sm–Nd isotopic study of a granulite domain in SE Madagascar. J Geol 102:523–538

Petrov GA (1995) Geology and geodynamic conditions for the forming of the Salda Metamorphic Complex (Middle Urals). In: Babansky AD, Bogatickov OA, Kovalenko VI, Pavlov VA, Puchkov VN, Rickus MV, Simon AK, Frolova TI (eds) Magmatism and geodynamics. Russian Academy of Science, Bashkortostan Republic Academy of Science, Ufa, pp 154–155 (in Russian)

Petrov GA, Borozdina GN (1996) New data on the geology of the Salda Metamorphic Complex (Middle Urals). In: Koroteev VA, Semikhatov MA, Maslov AV, Chuvashov BI, Heraskova TM, Ivanov KS, Fedonkin MA, Krupenin MT (eds) Vendian and Early Paleozoic palaeogeography. Uralian Section of Russian Academy of Science, Institute of Geology and Geochemistry, Ekaterinburg, pp 121–123 (in Russian)

Petrov GA, Shmelev VR, Karsten L, Friberg M (1998) New data on the geology and metamorphism of the Salda Complex (Middle Urals). In: Panjak SG (ed) Geology of metamorphic complexes. Urals state exploration geology academy, Ekaterineburg, pp. 41–54 (in Russian)

Petrov GA, Friberg M, Larionov AM, Schmelev VR (in press) Salda Metamorphic Complex: an example of subduction and collision related magmatism and metamorphism. Questions Geol Ore origin 1 (in Russian)

Potanin SD (1982) Gneiss domes of the eastern slopes of the Urals. Int Geol Rev 24:403–410

Sengör AMC, Natal'in BA, Burtman VS (1993) Evolution of the Altaid tectonic collage and Paleozoic crustal growth in Eurasia. Nature 364:299–307

Snelling NJ (1985) An interim time-scale. In: Snelling NJ (ed) The chronology of the geological record. Geol Soc Lond 10:261–265

Sobolev ID, Ananieva EM, Annenkova MN (1964) Geological map of the North, Middle and East part of South Urals, 1:500,000. Uralian Geological Committee, Sverdlovsk

Stacey JS, Kramers JD (1975) Approximation of terrestrial lead isotope evolution by a two-stage model. Earth Planet Sci Lett 26:207–221

Steiger RH, Jäger E (1978) Subcommission on geochronology: convention on the use of decay constants in geochronology and cosmochronology. In: Cohee GV, Glaessner MF, Hedberg HD (eds) Contributions to the geologic time scale. Studies in geology. American Association of Petroleum Geologists, Tulsa, pp 67–71

Tucker RD, McKerrow WS (1995) Early Paleozoic chronology: a review in light of new U–Pb zircon ages from Newfoundland and Britain. Can J Earth Sci 32:368–379

Zonenshain LP, Kuzmin MI, Kononov MV (1984) Absolute reconstruction of the Paleozoic oceans. Earth Planet Sci Lett 74:103–116